Available online at www.sciencedirect.com
ScienceDirect
Journal of Solid State Chemistry 180 (2007) 240–248
JOURNAL OF SOLID STATE CHEMISTRY
www.elsevier.com/locate/jssc

# Third- and second-order optical nonlinearity of Ge–Ga–S–$PbI_2$ chalcohalide glasses

Haitao Guo[a], Haizheng Tao[a], Shaoxuan Gu[a], Xiaolin Zheng[a], Yanbo Zhai[a,1], Saisai Chu[b], Xiujian Zhao[a,*], Shufeng Wang[b], Qihuang Gong[b]

[a]*Key Laboratory of Silicate Materials Science and Engineering, Ministry of Education, Wuhan University of Technology, Wuhan, Hubei 430070, PR China*
[b]*State Key Laboratory for Mesoscopic Physics & Department of Physics, Peking University, Beijing 100871, PR China*

Received 16 August 2006; received in revised form 13 October 2006; accepted 16 October 2006
Available online 21 October 2006

**Abstract**

Two series of metal iodide doped chalcohalide glasses $(100-2x)GeS_2 \cdot xGa_2S_3 \cdot xPbI_2$ $(0 \leqslant x \leqslant 20)$ and $(100-x)(0.8GeS_2 \cdot 0.2Ga_2S_3) \cdot xPbI_2$ $(0 \leqslant x \leqslant 15)$ were prepared and characterized. The microstructure of these glasses has been studied by Raman scattering spectra. Utilizing femtosecond time-resolved optical Kerr effect (OKE) technique at the wavelength of 820 nm, a largest third-order nonlinearity $\chi^{(3)}$ of $2.07 \times 10^{-13}$ esu was obtained for the $90GeS_2 \cdot 5Ga_2S_3 \cdot 5PbI_2$ glass, and it decreases with the addition of $PbI_2$ in both two series. After thermally poled, second-harmonic generation (SHG) has been observed in these glasses according to Maker fringe method and a large second-order nonlinearity $\chi^{(2)}$ as well as 4 pm/V was obtained for the $70GeS_2 \cdot 15Ga_2S_3 \cdot 15PbI_2$ glass. The variations of $\chi^{(2)}$ and $\chi^{(3)}$ on glass composition are ascribed to the evolution of micro-structural units in glass. These novel chalcohalide glasses would be expected to be the promising candidate materials for nonlinear optical devices.


*Keywords:* Chalcohalide glasses; Third-order optical nonlinearity; Second-order optical nonlinearity; Microstructure

## 1. Introduction

Nonlinear optical properties are currently under consideration for controlling signals in photonic systems. The nonlinear optical properties result from nonlinear electric polarization of materials, and the polarization, $P$, is expressed as a power series in the electric field, $E$, with

$$P = \varepsilon_0(\chi^{(1)}E + \chi^{(2)}E \cdot E + \chi^{(3)}E \cdot E \cdot E + \cdots) \quad (1)$$

where $\chi^{(1)}$ is the linear susceptibility, $\chi^{(2)}$ and $\chi^{(3)}$ are called the second- and third-order nonlinear susceptibilities, respectively. $\chi^{(3)}$ can be seen more or less in all materials, whereas $\chi^{(2)}$ can only be obtained in the materials with spatial inversion asymmetry.

As we know, future high-speed signal processing and high-bit rate telecommunications require high-speed switching devices. To develop ultrafast switch devices, it is desirable that the nonlinear optical medium possesses large $\chi^{(3)}$ and short response time. Compared with other third-order nonlinear optical materials such as organic polymers, inorganic homogeneous glasses have a long interaction length, high transparency, high thermal and chemical durability, etc. and seem to be more preferable for the viewpoints of ease of fabrication of fiber or waveguide. Therefore, many kinds of glasses having large third-order optical nonlinearity were studied and a variety of all-optical switching applications have been demonstrated. Oxide glasses containing heavy metal such as Bi, Pb, Tl, Nb, Ti have been widely investigated for optical nonlinearity as heavy-metal ions play an important role in enhancing the refractive indices of glasses [1–3]. In addition, chalcogenide and chalcohalide glasses, which

*Corresponding author. Fax: +86 27 87669729.
*E-mail addresses:* guoht_001@163.com (H. Guo), zhaoxj@public.wh.hb.cn (X. Zhao).
[1]Present Address: Zhejiang Academy of Building Research and Design, 28 Wener Road, Hangzhou, Zhejiang 310000, PR China.

0022-4596/$ - see front matter © 2006 Elsevier Inc. All rights reserved.
doi:10.1016/j.jssc.2006.10.012

possess the largest $\chi^{(3)}$ among inorganic glasses (about two or three orders of magnitude larger than that of silica) also called many researchers' attention to the mechanism and application. As- and Se-based glasses have been used in the optical switching devices due to their relatively high power densities, long interaction lengths, and strong nonlinearities [4–6]. However, these fibers may suffer from the large two-photon absorption (TPA) at telecommunication wavelengths of 1.3 and 1.55 μm and their application in all-optical devices is restricted [7].

On the other hand, materials with large $\chi^{(2)}$ have wide uses in the fields of high density data storage or spectral extension of laser sources. But for homogeneous glasses, $\chi^{(2)}$ should be zero because of their macroscopic inversion symmetry. Fortunately, when the glass is subjected to an appropriate external excitation field, the macroscopic optical anisotropy can be achieved as well as second harmonic generation (SHG). In 1986, Osterberg and Margulis [8] firstly reported that SHG were induced in $GeO_2$ doped $SiO_2$ glass fibers when subjected to 1.06 μm lasers. Later, in 1991, Myers et al. [9] demonstrated that SHG was derived in silica glass by thermal poling and the second-order susceptibility is as high as 1 pm/V or so. After that, more and more SHG phenomenon was observed in different glasses. Several explanations about the origin of the SHG have been put forward. One of the widely accepted ones [10] is that

$$\chi^{(2)} = \chi^{(3)} E_{dc}, \tag{2}$$

where $\chi^{(2)}$, $\chi^{(3)}$ are second- and third-order nonlinear susceptibility, respectively. $E_{dc}$ is the local direct-current electric field. According to this model, large SHG efficiencies can be expected to occur in chalcogenide and chalcohalide glasses due to their large refractive indices and large amount of structural defects to produce large $\chi^{(3)}$ and $E_{dc}$.

In this paper, we prepared some homogeneous glasses from the Ge–Ga–S–$PbI_2$ chalcohalide system. Their ultrafast third-order nonlinear optical responses are measured utilizing the femtosecond time-resolved optical Kerr effect (OKE) technique at the wavelength of 820 nm. On the other hand, second-order nonlinearities of the thermally poled glasses are studied using Maker fringe method. The glasses based on Ge–Ga–S system are chosen because of their wider transparency in the visible region and good thermal stability. Moreover, addition of heavy metal iodide $PbI_2$, in which Pb and I are both highly polarizable elements, can expect to get large third-order nonlinearity [11]. Based on the detailed structural analysis obtained from Raman spectra, interrelationships between the micro-structural units and the third-/second-order nonlinear optical properties were presented. Our work was aimed at the elucidation of the influence of glass composition on the third-/second-order nonlinearities in this novel chalcohalide system and a search of new material for efficient thermal/electrical induced SHG.

## 2. Experimental

### 2.1. Sample preparation

The investigated glasses were prepared by heating a mixture (typically 8 g) of required amounts of germanium (grains, 5N, Nanjing Germanium Co., Ltd. China), gallium (crushed pieces, 5N, SCRC Co., Ltd. China) and sulfur (powers, 5N, SCRC Co., Ltd. China) and lead iodide (powers, 3N, SCRC Co., Ltd. China) at 950 °C in an evacuated quartz ampoule (10 mm inner diameter ampoule) for 12 h. The liquid produced was quenched in a cold water bath and annealed for 2 h at 20–30 °C below their glass transition temperature. The obtained glasses were cut and polished to mirror smoothness with a thickness of 0.6 mm.

Thermal poling process was carried out as follows. The glass sample was sandwiched between two commercial borosilicate glass plates (0.15 mm in thickness) and contacted physically with cupreous electrodes. The commercial borosilicate glass plates were used to avoid contamination of copper which occurred on glass surfaces when the glass sample was contacted directly to the electrodes, and it is also effective to avoid discharge between the electrodes [12]. The glass sample sandwiched with the electrodes was put into a vessel filled with ethyl silicone oil and heated with electric furnace until to an aimed temperature ($T = 170$–$310$ °C; below the boiling point of ethyl silicone oil). After held at the temperature for 30 min, a dc field was applied for duration range of 5–90 min. Then the glass sample was removed from the furnace and cooled down to room temperature with the constant voltage applied. It is apparent that the actual voltage applied to the glass sample was less than the displayed voltage because the existence of the two commercial borosilicate glass plates.

### 2.2. Characterization

The compositions and uniformity of the obtained glasses were measured by electron probe microanalysis (EPMA) (JEOL JXA-8800R). The error of measurement is within $\pm 1\%$.

Raman measurement was conducted at room temperature using the back (180°) scattering configuration by the micro Raman Spectrometer (Renishaw RM-1000). For the avoidance of local laser damage that could easily occur under the microscope and could locally crystallize the amorphous samples, a He–Ne laser ($\lambda = 632.8$ nm) with a power less than 2.2 mW was used as an excitation source. The resolution of the Raman spectra was 1 $cm^{-1}$.

The UV–Vis–NIR absorption spectra of the samples were recorded using the Shimadzu UV-1601 spectroscopy system between 400 and 1100 nm wavelength at room temperature. Refractive indices were measured by using a Spectro-Ellipsometer (Woollam W-VASE) between 400 and 1300 nm wavelength at room temperature.

The ultrafast optical nonlinearity of the glass sample was measured using the optical Kerr effect (OKE) technique [13]. A laser pulse with 120 fs pulse duration at 820 nm operating at 76 MHz was regenerated from a Ti:sapphire laser (Mira 900F, Coherent, USA). The input beam of the laser was split into two parts: one beam was used as the pump beam, the other as the probe beam. The pump pulses induce transient birefringence in the nonlinear sample and cause the polarization change of the probe light. The intensity of the probe pulses is kept small compared to the pump pulses (ratio; 1:10). To avoid the saturation effect and the nonlinear absorption in the OKE, the pump power on the sample was set to be 200 mW in this experiment. The sample was positioned between a polarizer and an analyzer in a cross Nicole polarizer configuration. The polarization of the probe beam was rotated 45° with respect to the linear polarization of the pump beam. The OKE signals were detected by photomultiplier tube. The data were displayed and recorded by a personal computer that was also used to control the time delay between the pump and probe pulses by a stepping motor. Liquid $CS_2$ in a quartz cell with a thickness of 1.0 mm was used as a reference.

The SHG of thermally poled samples were characterized by the Maker fringe method [14]. The fundamental wave at 1064 nm of a pulsed Nd:YAG laser (Newwave Tempest 10 Hz) with a pulse width of ~10 ns was used as the incident light. The output light from the poled glass sample was passed through a prism to divide the SH wave with 532 nm from the fundamental wave. The SH wave was detected by a monochromator equipped with a photomultiplier. Polarization included *p* excitation and *p* detection. The output signal was accumulated by a boxcar integrator. The measurements were processed at various angles of incidence from −90° to 90°. The second harmonic intensity from a Z-cut quartz with thickness of 1.11 mm and $d_{11} = 0.36$ pm/V was also measured for the purpose of determining input light power and calculating second-order nonlinear optical coefficient of the samples.

## 3. Results and discussion

### 3.1. Composition change during synthesis

Analytical results obtained from EPMA and those calculated from the batch compositions of the $GeS_2$–$Ga_2S_3$–$PbI_2$ glasses are shown in Table 1. They reveal that the difference in composition because of the compositional fluctuation during synthesis between a batch and the glass sample was within reasonable range.

### 3.2. Glass structure

The separated bands by Gauss fit to the Raman spectrum of the $90GeS_2 \cdot 5Ga_2S_3 \cdot 5PbI_2$ glass are shown in Fig. 1. The bands of 340 and 150 $cm^{-1}$ are associated with the symmetrical stretching vibration ($\upsilon_1$) and asymmetrical bending vibration ($\upsilon_4$) modes of [$GeS_4$] tetrahedral, respectively, while the bands associated with the asymmetrical stretching vibration ($\upsilon_2$), symmetrical bending vibration ($\upsilon_3$) modes are too weak to be observed. The bands of 372, 432 and 388 $cm^{-1}$are associated with the vibrations of edge-shared [$GeS_4$] and [$GaS_4$] tetrahedral, respectively [15,16]. In addition, another four bands are ascribed to $PbI_2$ addition are also found. The small band at 113 $cm^{-1}$ is assigned to vibration of [$PbI_n$] ($n = 6$, 8, 10, 12) structural units. The band of 200 $cm^{-1}$ is associated with $\upsilon_1$ mode of [$S_3GeI$] and [$S_2GeI_2$] tetrahedra. The band of 232 $cm^{-1}$ is associated with $\upsilon_2$ mode of [$S_2GeI_2$] tetrahedra and the band of 256 $cm^{-1}$ is associated with $\upsilon_2$ mode of [$S_3GeI$] tetrahedra [17,18].

The Raman spectra of the $(100-2x)GeS_2 \cdot xGa_2S_3 \cdot xPbI_2$ ($x = 0$, 5, 10, 15, 20) glasses are shown in Fig. 2. The vibration intensity at 113 $cm^{-1}$ increases with the addition of $PbI_2$, which is associated with the formation of [$PbI_n$] ($n = 6$, 8, 10, 12) structural units. The increasing intensity at 232 $cm^{-1}$ indicates [$S_2GeI_2$] tetrahedra are gradually formed in network. The intensity at 256 $cm^{-1}$

Table 1
Experimental and calculated compositions of investigated $GeS_2$–$Ga_2S_3$–$PbI_2$ glasses

| Compositions (mol%) | Ge (at.%) | | Ga (at.%) | | S (at.%) | | Pb (at.%) | | I (at.%) | |
|---|---|---|---|---|---|---|---|---|---|---|
| | Exp. | Cal. | Exp. | Cal. | Exp. | Cal. | Exp. | Cal. | Exp. | Cal. |
| Series $(100-2x)GeS_2 \cdot xGa_2S_3 \cdot xPbI_2$ | | | | | | | | | | |
| $x = 0$ | 32.80 | 33.30 | — | — | 67.20 | 66.70 | — | — | — | — |
| $x = 5$ | 27.34 | 29.03 | 2.96 | 3.23 | 64.71 | 62.90 | 1.52 | 1.61 | 3.47 | 3.23 |
| $x = 10$ | 24.11 | 25.00 | 5.68 | 6.25 | 60.79 | 59.37 | 3.02 | 3.13 | 6.40 | 6.25 |
| $x = 15$ | 19.88 | 21.21 | 7.18 | 9.09 | 58.41 | 56.06 | 4.31 | 4.55 | 10.22 | 9.09 |
| $x = 20$ | 16.52 | 17.65 | 10.45 | 11.76 | 54.93 | 52.94 | 5.72 | 5.88 | 12.38 | 11.76 |
| Series $(100-x)(0.8GeS_2 \cdot 0.2Ga_2S_3) \cdot xPbI_2$ | | | | | | | | | | |
| $x = 0$ | 23.05 | 23.53 | 10.34 | 11.76 | 66.61 | 64.71 | — | — | — | — |
| $x = 2.5$ | 21.80 | 23.01 | 10.14 | 11.50 | 65.79 | 63.27 | 0.71 | 0.74 | 1.56 | 1.48 |
| $x = 5$ | 20.95 | 22.49 | 9.98 | 11.24 | 64.60 | 61.83 | 1.39 | 1.48 | 3.08 | 2.96 |
| $x = 10$ | 20.43 | 21.43 | 9.67 | 10.71 | 60.98 | 58.93 | 2.90 | 2.98 | 6.02 | 5.95 |
| $x = 15$ | 18.96 | 20.36 | 9.02 | 10.18 | 58.53 | 56.99 | 4.35 | 4.49 | 9.14 | 8.98 |

The error of compositional analysis is within ±1%.

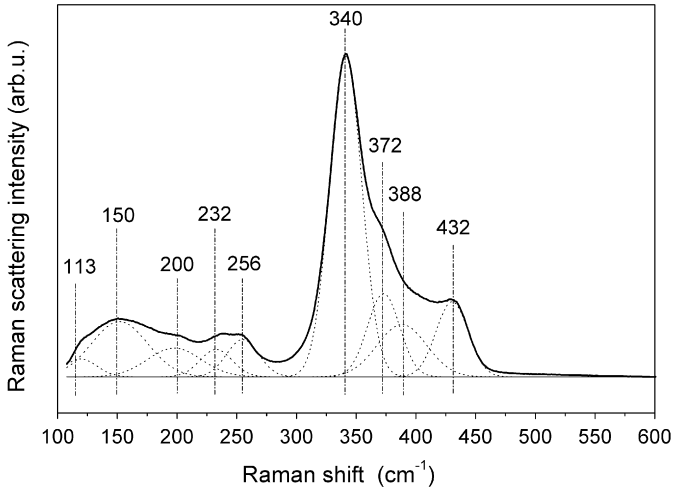


Fig. 1. Separated bands by Gauss fit to the Raman spectrum of the $90GeS_2 \cdot 5Ga_2S_3 \cdot 5PbI_2$ glass.

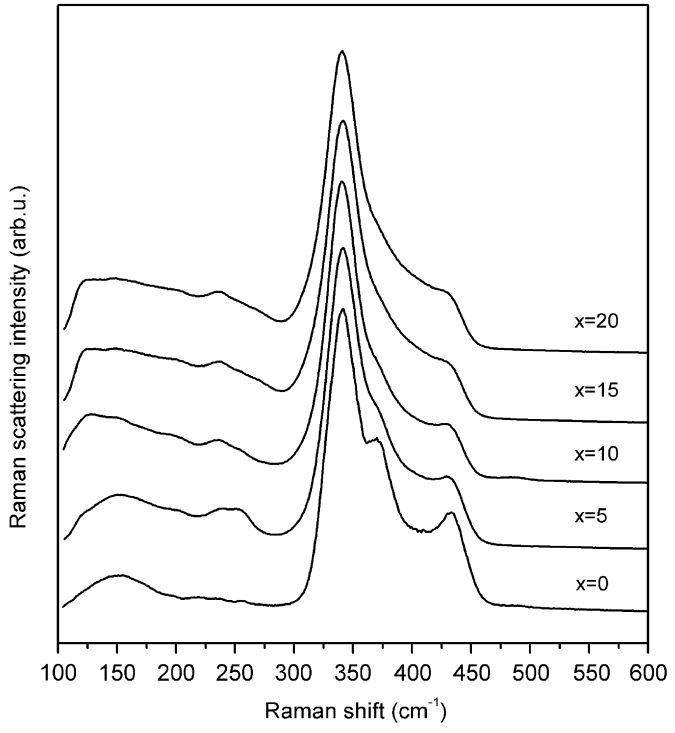


Fig. 2. Raman spectra of the $(100-2x)GeS_2 \cdot xGa_2S_3 \cdot xPbI_2$ ($x = 0$, 5, 10, 15 and 20) glasses.

which is assigned to the $[S_3GeI]$ tetrahedra does not increase; on the contrary, its intensity decreases when $x > 5$. This is assigned to the conversion from $[S_3GeI]$ to $[S_2GeI_2]$ tetrahedra because of the continuous addition of $PbI_2$.

The Raman spectra of another series $(100-x)(0.8GeS_2 \cdot 0.2Ga_2S_3) \cdot xPbI_2$ ($x = 0$, 2.5, 5, 10, 15) glasses are shown in Fig. 3. In this glass series, a band at $265\,cm^{-1}$ which is assigned to $\upsilon_3$ mode of ethane-like $[S_3(Ga)Ge–Ge(Ga)S_3]$ units [19] can be found in the glasses with low concentration of $PbI_2$. Because the S/Ga ratio for $Ga_2S_3$ is 1.5, which

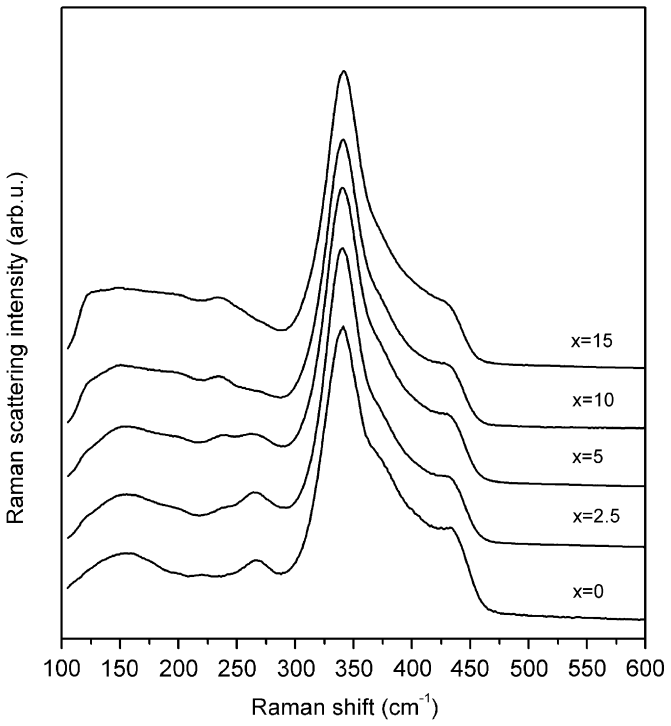


Fig. 3. Raman spectra of the $(100-x)(0.8GeS_2 \cdot 0.2Ga_2S_3) \cdot xPbI_2$ ($x = 0$, 2.5, 5, 10 and 15) glasses.

is less than 2 in the $[GaS_4]$ tetrahedra, formation of $[GaS_4]$ tetrahedra from $Ga_2S_3$ will lead to the deficiency of sulfur in glasses. Then the emergence of the ethane-like $[S_3(Ga)$-$Ge–Ge(Ga)S_3]$ units can compensate for the shortage of sulfur in glass net. With the addition of $PbI_2$, the intensity at $265\,cm^{-1}$ decreases obviously and shrinks to nothing when $x \geqslant 10$. This is due to the substituting of iodine atoms to sulfur atoms in original $[GeS_4]$ tetrahedra forms $[S_{4-x}GeI_x]$ ($x = 1$, 2) tetrahedra and thus alleviates the S-deficiency of a number of Ge–Ge/Ga–Ga bonds. Finally, a distinct increase of intensity at $232\,cm^{-1}$ is also observed, which indicates the $[S_2GeI_2]$ tetrahedra are aboundantly formed in glass net.

Based on the above results of Raman spectra, we can conclude that the introduction of $PbI_2$ played two main roles in this system. Firstly, some $[PbI_n]$ ($n = 6$, 8, 10, 12) structural units, mixed-anion tetrahedra $[S_3GeI]$ and $[S_2GeI_2]$ are abundantly formed. Because of the chain-terminating function of iodine, these new structural units will break down the connectivity of the original glass net. Secondly, the substitution process of ions $I^-$ for ions $S^{2-}$ alleviates the sulfur shortage in glass and remarkably reduces the amount of ethane-like $[S_3(Ga)Ge–Ge(Ga)S_3]$ units.

### 3.3. Absorption spectroscopy and refractive indices

Fig. 4 shows the optical linear absorption spectrum of the $76GeS_2 \cdot 19Ga_2S_3 \cdot 5PbI_2$ glass in the Visible and near-IR region (Vis–NIR). It indicates that there is almost no

absorption at a laser wavelength of 820 nm. The absorption spectra of all samples are very similar to each other except for minor shifts of the absorption edge, which correspond to respective optical bandgap ($E_g$). The values of absorption-edges are listed in Table 2. As can be seen, when $PbI_2$ content increases, the optical absorption-edge shifts to the long-wavelength region gradually. This can be ascribed that $I^-$ ion has comparable elecronegativity but larger ionic radius than $S^{2-}$ ion and $Pb^{2+}$ ion has loose electronic shell and $6S^2$ outermost electron. So, with the addition of $PbI_2$, the $E_g$ of glass decreases, which corresponds to a red-shift of the visible absorption edge.

The data of the refractive indices of glasses at laser wavelengths 820, 1064 and 532 nm are summarized in Tables 2 and 3, which are used in calculation of third-order nonlinear susceptibility and second-order nonlinear susceptibility, respectively. The refractive indices are relatively high, which is rather beneficial for promising applications in all-optical devices. Furthermore, with the addition of $PbI_2$, the refractive index increases monotonously, which is expected in view of the increasing packing density and the larger polarizability of $Pb^{2+}$ ions in comparison with $Ge^{4+}$ ones.

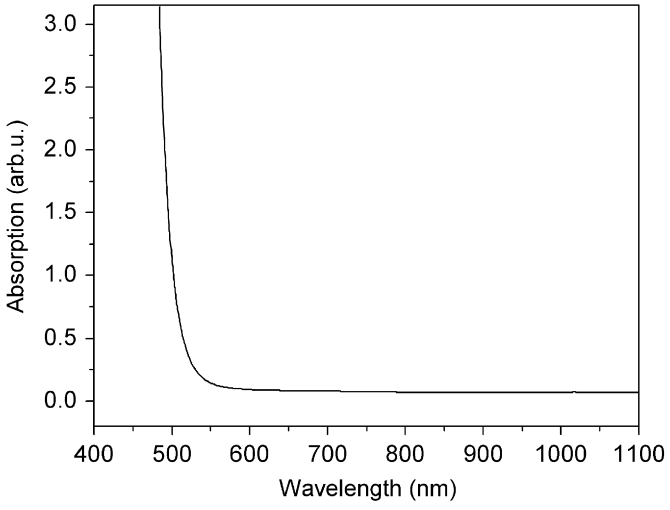


Fig. 4. Absorption spectrum of the $76GeS_2 \cdot 19Ga_2S_3 \cdot 5PbI_2$ glass.

### 3.4. Third-order optical nonlinearity

Fig. 5 shows the optical Kerr signal of the standard $CS_2$ reference medium at a wavelength of 820 nm. The $CS_2$ medium has an asymmetrical decay tail with over 1 ps response originating from the molecular reorientation relaxation processes, i.e., the nuclear response. Under the same experimental conditions, the glass samples were substituted for $CS_2$ and some of the typical experimental results are shown in Fig. 6. The temporal profile of the Kerr signal in these samples is symmetrical (Gaussian shape) with the full width at half maximum of 180 fs.

Using the standard procedure of reference measurement, the value of third-order optical nonlinear susceptibility, $\chi^{(3)}$, of the sample can be calculated by the following equation [20]:

$$\chi_S^{(3)} = \chi_R^{(3)} \left(\frac{I_S}{I_R}\right)^{1/2} \left(\frac{n_S}{n_R}\right)^2, \quad (3)$$

where the subscripts S and R refer to the glass sample and the reference ($CS_2$), respectively, $I$ is the intensity of the obtained optical Kerr signal, and $n$ is the linear refractive index. The $n$ of $CS_2$ is 1.62 and its nonlinear refractive index, $n_2$, is $3 \times 10^{-12}$ esu in femtosecond time scale [21]. Since the relation between $n_2$ in esu and $\chi^{(3)}$ in esu is given by $n_2 = 12\pi\chi^{(3)}/n$ for isotropic media, the $\chi^{(3)}$ of $CS_2$ is then estimated to be $1.3 \times 10^{-13}$ esu. To determine the value of $\chi^{(3)}$, we use the maximum values of the optical Kerr signals of the sample and $CS_2$ before normalization. The values of OKE, i.e. $I_S/I_R$ and the calculated $\chi^{(3)}$ of the sample at 820 nm are listed in Table 2. According to Eq. (3), a maximum optical nonlinearity $\chi^{(3)}$ of the $90GeS_2 \cdot 5Ga_2S_3 \cdot 5PbI_2$ glass is calculated to be as well as $2.07 \times 10^{-13}$ esu at 820 nm within an estimated error of

Table 2
Some fundamental parameters and third-order optical nonlinearities of the examined glass samples in the $GeS_2$–$Ga_2S_3$–$PbI_2$ system

| Composition (mol%) | Absorption edge[a] (nm) | $n$ (at 820 nm) | OKE[b] (at 820 nm) | $\chi^{(3)}$ ($10^{-13}$ esu) | $n_2$ ($10^{-15}$ cm$^2$/W) |
|---|---|---|---|---|---|
| Series $(100-2x)GeS_2 \cdot xGa_2S_3 \cdot xPbI_2$ | | | | | |
| $x = 5$ | 525 | 2.10 | 0.90 | 2.07 | 7.21 |
| $x = 10$ | 539 | 2.16 | 0.76 | 2.01 | 6.81 |
| $x = 15$ | 550 | 2.17 | 0.67 | 1.91 | 6.43 |
| $x = 20$ | 558 | 2.19 | 0.42 | 1.67 | 5.14 |
| Series $(100-x)(0.8GeS_2 \cdot 0.2Ga_2S_3) \cdot xPbI_2$ | | | | | |
| $x = 2.5$ | 506 | 2.05 | 0.65 | 1.68 | 5.98 |
| $x = 5$ | 518 | 2.09 | 0.60 | 1.68 | 5.86 |
| $x = 10$ | 536 | 2.17 | 0.51 | 1.67 | 5.61 |
| $x = 15$ | 550 | 2.23 | 0.20 | 1.09 | 3.61 |

[a]Absorption edge is the wavelength where the transmission is 50% of that at 1000 nm and the error is ±2 nm.
[b]OKE represents the ratio of Kerr signal intensity of glass samples to that of $CS_2$, i.e. $I_S/I_R$.

Table 3
Some fundamental parameters and second-order optical nonlinearities of the examined glass samples in the $(100-2x)GeS_2 \cdot xGa_2S_3 \cdot xPbI_2$ system

| Composition (mol%) | $n_\omega$ (at 1064 nm) | $n_{2\omega}$ (at 532 nm) | $l_c$ (μm) | Poling conditions | $\chi^{(2)}$ (pm/V) |
|---|---|---|---|---|---|
| $x = 5$ | 2.18 | 2.06 | 2.83 | 270 °C, 6 kV, 40 min | 0.35 |
| $x = 10$ | 2.23 | 2.12 | 2.53 | 290 °C, 6 kV, 40 min | 2.17 |
| $x = 15$ | 2.26 | 2.15 | 2.35 | 250 °C, 6 kV, 40 min | 3.99 |
| $x = 20$ | 2.29 | 2.16 | 2.15 | 230 °C, 6 kV, 40 min | 3.32 |

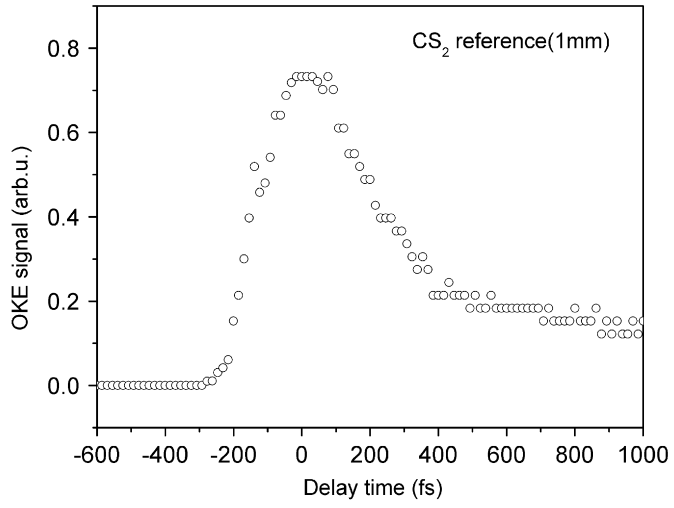


Fig. 5. Time-resolved optical Kerr signal of Standard $CS_2$ reference medium.

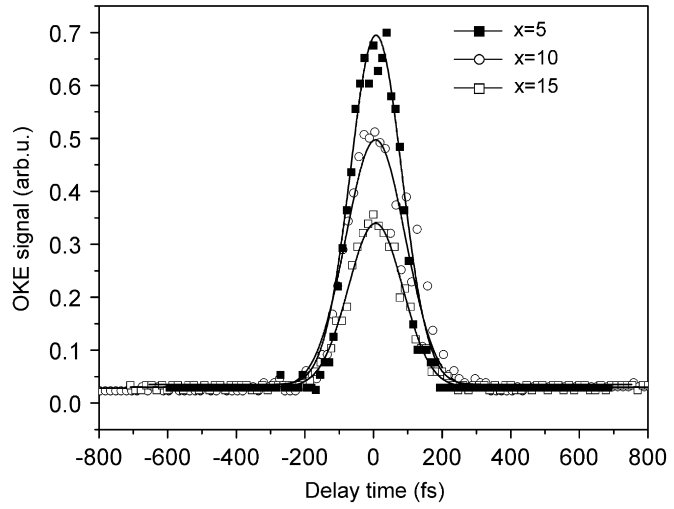


Fig. 6. Time-resolved optical Kerr signal of the $(100-2x)GeS_2 \cdot xGa_2S_3 \cdot xPbI_2$ ($x = 5$, 10 and 20) glasses at a wavelength of 820 nm.

10%. The nonlinear refractive index $n_2$ value is then estimated to be $7.21 \times 10^{-15}\,cm^2/W$. These values are higher compared with other optical Kerr shutter (OKS) glasses [22,23].

For the glass materials, the ultrafast third-order nonlinear optical responses originate from the distortion of electron cloud or the motion of nuclei. The former has a response time less than 10 fs and the latter has a relaxation time lying between 100 fs and 10 ps. In our experiment, the pulse duration is 180 fs and the nuclear optical nonlinear contributions cannot be resolved. However, the nuclear optical nonlinear contribution is much smaller than the electronic part [24]. Therefore, it can be deduced that the third-order nonlinear responses of the Ge–Ga–S–$PbI_2$ chalcohalide glasses are produced dominantly by the electronic contribution.

According to Table 2, it reveals that the ratio of intensity of Kerr signals for the present glasses and the reference $CS_2$ decreases with the increased concentration of $PbI_2$ within the Ge–Ga–S–$PbI_2$ chalcohalide glasses. This phenomenon is different from previous results about the $As_2S_3$–$Sb_2S_3$–$PbI_2$ system [11]. We assume that the change of microstructural units lead to the decrease of intensity of Kerr signal. On the basis of above structural analysis, with the addition of $PbI_2$, the amount of original $[GeS_4]$ tetrahedra decreases whereas the number of $[S_{4-x}GeI_x]$ ($x = 1$, 2) tetrahedra in the glass net becomes larger. Kang et al. [25] have investigated the nuclear optical nonlinear contribution of a Ge–Ga sulfide glass using Z-scan technique with a 35 fs laser and revealed that a damped ultrafast oscillatory response with a period of 98 fs originated from the $\upsilon_2$ breathing Raman mode of the $[GeS_4]$ tetrahedra. This reveals that the $[GeS_4]$ tetrahedra play an important role in the ultrafast third-order nonlinear optical responses of these chalcohalide glasses and it suggests that the ultrafast third-order nonlinear optical responses mainly originate from the virtual electronic transition between the conduction and valence bands formed by the bonding and antibonding orbits of Ge–S. Simultaneously, $[S_{4-x}GeI_x]$ ($x = 1$, 2) structural units have negative effect to the ultrafast third-order optical nonlinearity. It can be also deduced ulteriorly that the integrated and ordered glass network without structural defects is more beneficial to the enhancement of third-order optical nonlinearity.

According to Miller's rule [26], it is possible to estimate the third-order nonlinear susceptibility, $\chi^{(3)}$, of a material from the refractive index, $n$:

$$\chi^{(3)} = \left(\frac{n^2-1}{4\pi}\right)^4 \times 10^{-10}. \quad (4)$$

It can be deduced that larger $n$ can induce larger $\chi^{(3)}$. From the results in Table 2, the $n$ increases with the addition of $PbI_2$ while the value of $\chi^{(3)}$ decreases reversely, this indicates that the femtosecond time resolved third-order optical nonlinear responses of the Ge–Ga–S–$PbI_2$ glasses do not obey the semiempirical Miller's rule. And the structural units play a more important role in the variation of third-order optical nonlinearity with composition in this system.

### 3.5. Second-order optical nonlinearity

Fig. 7 shows a characteristic Maker fringe pattern of the thermally poled $70GeS_2 \cdot 15Ga_2S_3 \cdot 15PbI_2$ glass sample poled at 250 °C under 6.0 kV for 40 min. The inset shows the Maker fringe of unpoled sample. It is clear that thermally poled glass sample is SHG-active, while unpoled glass does not show any SHG activity. Simultaneously, the obtained Maker fringe pattern has good symmetry and maximum of second-harmonic intensity appear at the incident angle of $\pm 60°$.

No obvious changes are observed under optical microscopy between the unpoled glass and the poled one. Therefore, the electrochemical reaction on the glass surfaces should not be serious at all. To check that such a Maker fringe pattern comes from a thin nonlinear layer at the anodic surface of the poled glass, we have polished this surface by 0.05 mol/L concentration KOH solution that a thickness of 10 μm was etched. After this processing, no obvious SH signal except some little noise could be detected, which indicates that the thickness of the poled region at the anodic surface is less than 10 μm.

Table 3 summarizes the values of the refractive indices at 1064 and 532 nm ($n_\omega$ and $n_{2\omega}$), the corresponding coherence length $l_c$, optimal poling conditions (including poling temperature, dc voltage and duration) for each sample, second-order susceptibility $\chi^{(2)}$ obtained under optimal poling condition and mole percent $x$. A curve between $\chi^{(2)}$ and mole percent $x$ can be got as shown in Fig. 8, together with the dependence of third-order susceptibility $\chi^{(3)}$ on mole percent $x$. Second-order susceptibility $\chi^{(2)}$ shows an increase first and then decrease with the increasing $PbI_2$ content. A maximum $\chi^{(2)}$, 4 pm/V, can be obtained when $x = 15$, i.e., $70GeS_2 \cdot 15Ga_2S_3 \cdot 15PbI_2$ glass after optimal poling. Fig. 8 shows that $\chi^{(2)}$ and $\chi^{(3)}$ have almost reverse variation trends. According to Eq. (2), the relationship of $\chi^{(2)}$ and $\chi^{(3)}$ should be expressed as $\chi^{(2)} \propto \chi^{(3)} E_{dc}$, therefore it is seems that the $E_{dc}$ is different in each composition glass after poled.

Recently, Nakane et al. [27] reported their research in thermally poled $GeS_x$ ($x = 3$, 4, 5, 6) glass system. By comparing Raman scattering measurement before and after poling, structure deformation, mainly the breaking of weak S–S homopolar bonds, is ascribed to second harmonic generation in it. In our experiment, the Raman spectra of Ge–Ga–S–$PbI_2$ glass samples before and after poling are also measured and the composition of $70GeS_2 \cdot 15Ga_2S_3 \cdot 15PbI_2$ is taken as an example (in Fig. 9). No marked structural modification, including vibration intensities and situations of peaks, can be found on either the anodic surface or the cathodic surface. Considering the low concentration of the weaker homopolar S–S or Ge–Ge/Ga–Ga bonds and large amount of stronger bonds in this glass system, no observation of similar structure modification can be understood.

Actually, chalcogenide and chalcohalide glasses always contain large amounts of defects and Seki et al. [28,29] affirmed the presence of electric dipoles in Ge–S glass by researching its photoluminescence property. As for Ge–Ga–S–$PbI_2$ glass, larger amounts of Ge–S, Ga–S, Ge–I and Pb–I electric dipoles are present in the structure. The orientation of dipoles under dc field is taken into account to explain the SHG and the increase of complex anion $[S_{4-x}GeI_x]$ ($x = 1$, 2) units especially the $[S_2GeI_2]$ ones with

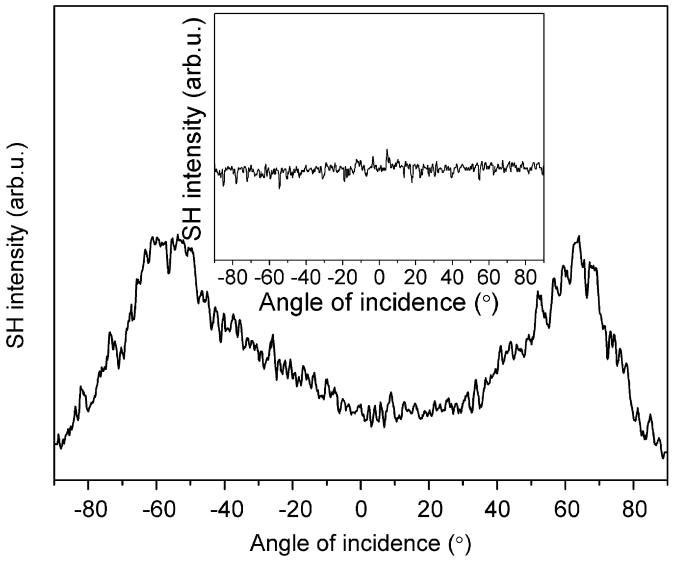


Fig. 7. Maker fringe pattern of the $70GeS_2 \cdot 15Ga_2S_3 \cdot 15PbI_2$ glass poled at 250 °C under 6.0 kV for 40 min. The inset shows the Maker fringes of as-prepared glass.

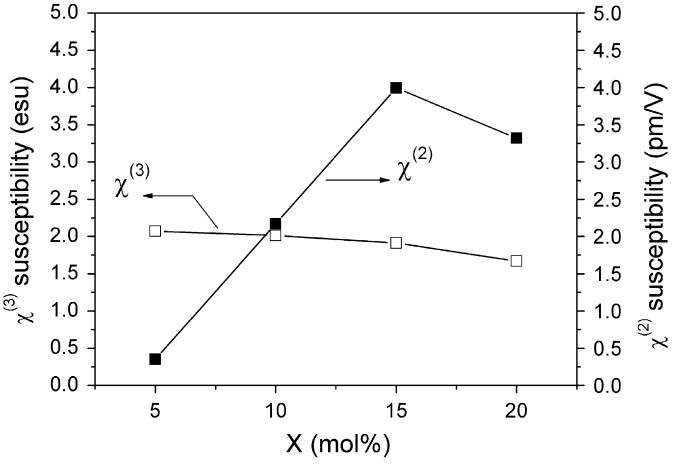


Fig. 8. Second-order susceptibility $\chi^{(2)}$ and third-order susceptibility $\chi^{(3)}$ of the $(100-2x)GeS_2 \cdot xGa_2S_3 \cdot xPbI_2$ ($x = 5$, 10, 15 and 20) glasses.

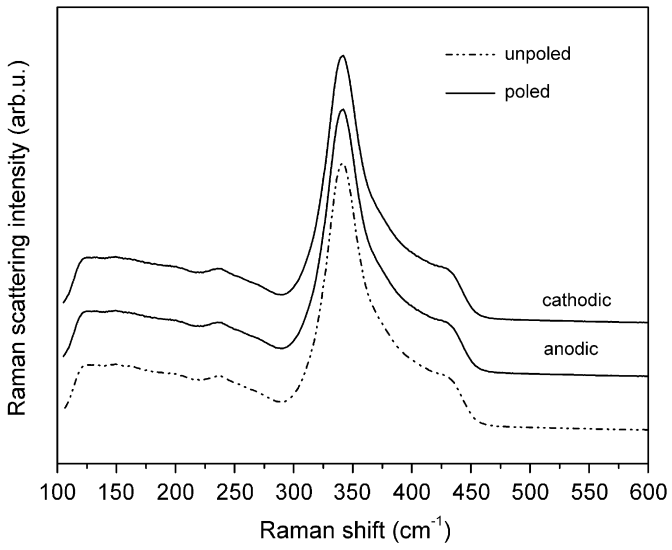


Fig. 9. Comparison of Raman spectra of the $70GeS_2 \cdot 15Ga_2S_3 \cdot 15PbI_2$ glass before and after poled at 250 °C under 6.0 kV for 40 min. The 'anodic' and 'cathodic' mean the detected glass surfaces after poled.

the addition of $PbI_2$ is considered responsible for the dependence of $\chi^{(2)}$ on glass composition.

Firstly, the orientation of polarizable dipoles is a solid state chemistry approach, the germanium iodine bonds are more ionic than the germanium sulfur bonds which make orientation of the $[S_{4-x}GeI_x]$ ($x = 1, 2$) tetrahedral easier especially the $[S_2GeI_2]$ ones by applying the dc field. Secondly, because of the chain-terminating function of iodine, addition of $PbI_2$ decreases the connectivity of structural units and thus increases the structure flexibility. This enhances the amount of the dipoles which have enough activation energy to break the bondage of glass net. These above two factors lead to the increase of second-order nonlinearity $\chi^{(2)}$ when the mole percent $x \leqslant 15$. However, on the contrary, excessive loose glass structure makes the dipoles vibrate more vigorously, which causes the inner frozen-in process hard to be realized [30]. So, continuous addition of $PbI_2$ when mole percent $x \geqslant 15$ has a negative effect on the second-order susceptibility $\chi^{(2)}$. Moreover, because of the different amount of orientated dipoles in each poled composition glass, the local direct-current electric field, i.e., $E_{dc}$ is different, and thus leads to different variation trends of $\chi^{(2)}$ and $\chi^{(3)}$ in $\chi^{(2)} \propto \chi^{(3)} E_{dc}$. Our experiment reveals that addition of heavy metal iodides such as $PbI_2$ into the glasses can effectively improve the SHG but its concentration should be optimized.

## 4. Conclusion

For searching novel materials with potential practical applications in the field of optoelectronics, two series of metal iodide doped chalcohalide glasses $(100-2x)GeS_2 \cdot xGa_2S_3 \cdot xPbI_2$ ($0 \leqslant x \leqslant 20$) and $(100-x)(0.8GeS_2 \cdot 0.2Ga_2S_3) \cdot xPbI_2$ ($0 \leqslant x \leqslant 15$) were elaborated. The structural organizations of the two series and their evolutions induced by the addition of $PbI_2$ have been investigated by Raman scattering spectra. The linear and nonlinear optical properties have also been characterized. Significant growth of linear refractive indices with increasing concentration of $PbI_2$ was recorded. For third-order nonlinear susceptibility $\chi^{(3)}$, increase of $PbI_2$ has no obvious positive effect, the largest $\chi^{(3)}$ was estimated to be $2.07 \times 10^{-13}$ esu at 820 nm for the $90GeS_2 \cdot 5Ga_2S_3 \cdot 5PbI_2$ glass. This value is high enough in comparison with those of heavy-metal oxide glasses and some chalcogenide glasses. After effectively poled under dc field, SHG in $(100-2x)GeS_2 \cdot xGa_2S_3 \cdot xPbI_2$ ($0 \leqslant x \leqslant 20$) glasses was observed and an expectedly large second-order nonlinearity $\chi^{(2)}$ as well as 4 pm/V was obtained for $x = 15$, i.e. $70GeS_2 \cdot 15Ga_2S_3 \cdot 15PbI_2$ glass. Based on structural analysis, it is suggested that the $[GeS_4]$ tetrahedra play an important role in the ultrafast third-order nonlinear optical responses of these chalcohalide glasses, while orientation of the $[S_{4-x}GeI_x]$ ($x = 1, 2$) tetrahedra especially the $[S_2GeI_2]$ ones by applying the dc field and structural relaxation causing by $PbI_2$ addition are responsible for the SHG and the variation of $\chi^{(2)}$ on the glass compositions.

## Acknowledgment

This work was partially funded by the National Natural Science Foundation of China (No. 50125205), the Opening Fund of Key Laboratory of Silicate Materials Science and Engineering (Wuhan University of Technology) Ministry of Education (No. SYSJJ2004-14).

## References

[1] H. Nasu, J. Matsuoka, K. Kamiya, J. Non-Cryst. Solids 178 (1994) 23.
[2] H. Nasu, T. Ito, H. Hase, J. Matsuoka, K. Kamiya, J. Non-Cryst. Solids 204 (1996) 78.
[3] S. Smolorz, I. Kang, F. Wise, B.G. Aitken, N.F. Borrelli, J. Non-Cryst. Solids 256&257 (1999) 310.
[4] M. Asobe, T. Kanamori, K. Kubodera, IEEE J. Quantum. Electron. 29 (1993) 2325.
[5] M. Asobe, Opt. Fiber Technol. 3 (1997) 142.
[6] J.M. Harbold, F.O. Ilday, F.W. Wise, B.G. Aitken, IEEE Photon. Technol. Lett. 14 (2002) 822.
[7] K. Ogusu, J. Yamasaki, S. Maeda, M. Kitao, M. Minakata, Opt. Lett. 29 (2004) 265.
[8] U. Osterberg, W. Margulis, Opt. Lett. 11 (1986) 516.
[9] R.A. Myers, N. Mukherjee, S.R.J. Brueck, Opt. Lett. 16 (1991) 1732.
[10] D.Z. Anderson, et al., Opt. Lett. 16 (1991) 796.
[11] J. Troles, F. Smektala, G. Boudebs, A. Monteil, Opt. Mater. 22 (2003) 335.
[12] A. Narazaki, K. Tanaka, K. Hirao, N. Soga, J. Appl. Phys. 83 (1998) 3987.
[13] Q.H. Gong, J. Li, T. Zhang, H. Yang, Chin. Phys. Lett. 15 (1998) 30.
[14] P.D. Maker, R.W. Terhune, M. Nisenoff, C.M. Savage, Phys. Rev. Lett. 8 (1962) 21.
[15] S. Sugai, Phys. Rev. B 35 (1987) 1345.
[16] P.M. bridenbaugh, G.P. Espinosa, J.E. Griffiths, J.C. Philips, J.P. Remeika, Phys. Rev. B 20 (1979) 4140.
[17] L. Koudelka, M. Pisárčik, J. Non-Cryst. Solids 113 (1989) 239.
[18] J. Heo, J.D. Mackenzie, J. Non-Cryst. Solids 113 (1989) 246.

[19] J. Heo, J.M. Yoon, S.Y. Ryou, J. Non-Cryst. Solids 238 (1998) 115.
[20] M.K. Casstevens, M. Samoc, J. Pfleger, P.N. Prasad, J. Chem. Phys. 92 (1990) 2019.
[21] K. Minoshima, M. Taiji, T. Kobayashi, Opt. Lett. 16 (1991) 1683.
[22] S. Kinoshita, H. Ozawa, Y. Kanematsu, et al., Rev. Sci. Instrum. 71 (2000) 3317.
[23] D.W. Hall, M.A. Newhouse, N.F. Borrelli, W.H. Dumbaugh, D.L. Weidman, Appl. Phys. Lett. 54 (1989) 1293.
[24] J.E. Aber, M.C. Newstein, B.A. Garetz, J. Opt. Soc. Am. B 17 (2000) 120.
[25] I. Kang, S. Smolorz, T. Krauss, F. Wise, B.G. Aitken, N.F. Borrelli, Phys. Rev. B. 54 (1996) 12641.
[26] R.C. Miller, Appl. Phys. Lett. 5 (1964) 17–19.
[27] Y. Nakane, H. Nasu, J. Heo, T. Hashimoto, K. Kamiya, J. Ceram. Soc. Jpn. 113 (11) (2005) 728.
[28] M. Seki, K. Hachiya, K. Yoshida, J. Non-Cryst. Solids 315 (2003) 107.
[29] M. Seki, K. Hachiya, K. Yoshida, J. Non-Cryst. Solids 324 (2003) 127.
[30] K. Tanaka, A. Narazaki, K. Hirao, N. Soga, J. Appl. Phys. 79 (1996) 3798.